Biomaterials 185 (2018) 360–370

Contents lists available at ScienceDirect

Biomaterials

journal homepage: www.elsevier.com/locate/biomaterials

Bioengineered stem cell membrane functionalized nanocarriers for therapeutic targeting of severe hindlimb ischemia

Rajendran JC. Bose[a,b,e,f,1], Byoung Ju Kim[b,g,1], Yoshie Arai[b,g], In-bo Han[c], James J. Moon[d], Ramasamy Paulmurugan[e,f], Hansoo Park[a,**], Soo-Hong Lee[b,g,*]

[a] Advanced Biomaterials and Stem Cell Engineering Laboratory, School of Integrative Engineering, Chung-Ang University, 84 Heuk Seok-Ro, Dongjak-Gu, Seoul, South Korea
[b] Stem Cell Engineering Laboratory, Department of Biomedical Science, CHA University, Pangyo-Ro 335, Bundang-gu, Seongnam-si, Gyeonggi-do 463-400, South Korea
[c] Department of Neurosurgery, CHA University, Pangyo-Ro 335, Bundang-gu, Seongnam-si, Gyeonggi-do 463-400, South Korea
[d] Department of Pharmaceutical Sciences, Department of Biomedical Engineering & Biointerfaces Institute, University of Michigan, Ann Arbor, MI 48109, USA
[e] Molecular Imaging Program at Stanford (MIPS), and Bio-X Program, Department of Radiology, School of Medicine, Stanford University, Stanford, CA, 94305-5427, USA
[f] Canary Center at Stanford for Cancer Early Detection, Department of Radiology, School of Medicine, Stanford University, CA, 94305-5427, USA
[g] Stem Cells Integrative Engineering Laboratory, Department of Medical Biotechnology, Dongguk University, 32 Dongguk-ro, Ilsandong-gu, Goyang-si, Gyeonggi-do, 10326, South Korea

ARTICLE INFO

Keywords:
Bioengineered stem cell membrane nanocarriers
CXCR4
Endothelial cell barrier
Phagocyte uptake
Hindlimb ischemia
PLGA nanoparticle

ABSTRACT

Bioengineering strategies to enhance the natural targeting function of nanocarriers would expand their therapeutic applications. Here, we designed bioengineered stem cell membrane-functionalized nanocarriers (BSMNCs) harboring C-X-C chemokine receptor type 4 (CXCR4) to achieve robust targeting and also to increase their retention time in ischemic tissue. Stem cell membrane coated nanocarrier (SMNCs) or poly (lactic-*co*-glycolic acid) (PLGA) nanocarriers (PNCs) and BSMNCs were prepared by functionalizing PNCs with human adipose-derived stem cells (hASCs) membranes and hASCs engineered to overexpress CXCR4-receptor, respectively. The functionalization of PNCs with stem cell membranes derived from hASCs significantly enhance the nanocarrier penetration across endothelial cell barrier compare to PNCs. In addition, stem cell membrane functionalization on PNCs also significantly decreased the nanoparticles uptake in J774 (murine) and THP (human) macrophages respectively from 84% to 76%–29% and 24%. Interestingly, BSMNCs showed much higher level of accumulation in ischemic tissue than SMNCs. Systemic retro-orbital injection of BSMNCs loaded with VEGF into mice with hindlimb ischemia resulted substantially enhancement of blood reperfusion, muscle repair, and limb salvage compared to animals treated with SMNCs loaded with similar concentration of VEGF. The reported strategy could be used to create biocompatible and custom-tailored biomimetic nanoparticles with various hybrid functionalities, which may overcome the limitations of current nanoparticle-based therapeutic and imaging platforms.

1. Introduction

Critical limb ischemia (CLI) is a severe form of peripheral arterial disease associated with high morbidity and mortality [1]. Unfortunately, current surgical procedures or endovascular revascularization cannot offer a cure for many patients, largely due to the intricate anatomy of the vascular occlusion and other risk factors [2]. Recent findings indicated that non-invasive stem cell therapy holds great promise for the treatment of CLI [3–5]. Yellowley et al. showed that the ischemic tissue-directed homing response of mesenchymal stem cells (MSCs) is mediated by interactions between C-X-C chemokine receptor type 4 (CXCR4) expressed on MSCs and stromal-derived factor (SDF), a chemokine, secreted by injured tissues [6]. Genetic engineering approaches have been used to further improve stem cell migration and homing to sites of injury [7,8]. However, numerous challenges must be overcome before stem cell therapies can be successfully applied to CLI.

* Corresponding author. Stem Cell Engineering Laboratory, Department of Biomedical Science, CHA University, Pangyo-Ro 335, Bundang-gu, Seongnam-si, Gyeonggi-do 463-400, South Korea.
** Corresponding author.
E-mail addresses: heyshoo@cau.ac.kr (H. Park), soohong@dongguk.edu (S.-H. Lee).
[1] These authors contributed equally to this work.

https://doi.org/10.1016/j.biomaterials.2018.08.018
Received 30 April 2018; Received in revised form 31 July 2018; Accepted 6 August 2018
Available online 09 August 2018
0142-9612/

In particular, issues related to cell product scalability and reproducibility, as well as the challenge of the longitudinal monitoring of stem cell fate *in vivo,* must be resolved before this technique can be used for broad clinical applications [9–12].

Cell membrane-functionalized nanocarriers (CMNCs) have the potential to address many of the shortcomings of cell therapy and pave the way for therapeutic options that are more effective and safer than stem cell therapy alone [13–15]. Recently, red blood cells (RBCs) and platelets have been investigated as source materials for preparation of CMNCs [13]. However, their membranes may not have all the functional biomolecules required for efficient targeting to specific tissues [16] and also lack engineering options to specifically customize the cells for particle preparations. Furthermore, the large number of cells required for the preparation of CMNCs and the practical difficulties of genetic engineering are major factors that limit the clinical applications of CMNCs prepared from RBCs or platelets [13,16,17]. Therefore, novel strategies are required to improve the functional capability of CMNCs. Recently several bioengineering strategies have been demonstrated to enhance the functionality of cell derived materials [18,19].

In this study, we designed bioengineered stem cell membrane-coated nanocarriers (BSMNCs) using bioengineered stem cell membranes, with the goal of improving targeted delivery to ischemic hindlimbs. To take advantage of the unique CXCR4-mediated stem cell tropism, we engineered human adipose-derived stem cells (hASCs) to overexpress CXCR4 on the membrane (CXCR4-hASCs) and used for coating vascular endothelial growth factor (VEGF)-loaded poly (lactic-*co*-glycolic acid) (PLGA) nanocarriers (PNCs) with these membranes. Here, we report our plasma membrane isolation procedure that allowed for the CXCR4 receptors remain embedded in the engineered hASCs membrane of the resultant vesicles and maintain the structural integrity of receptors, allowing targeting ligands for stromal cell-derived factor-1 (SDF-1), thereby enhancing targeted delivery of VEGF [20]. As a control, we also prepared non-engineered stem cell membrane-coated nanocarriers (SMNCs) using non-engineered hASC membranes.

2. Materials and methods

2.1. Materials

PLGA (50:50) (Resomer® RG 502 H, molecular weight 7000–17,000) was purchased from Sigma–Aldrich Co (St Louis, MO, USA). Fluorescent lipid 1-oleoyl-2-[12-[(7-nitro-2-1,3-benzoxadiazol-4-yl) amino]dodecanoyl]-*sn*-glycero-3-phosphocholine] (NBD-PC) was purchased from Avanti Polar Lipids (Alabaster, AL, USA). 1, 1′-dioctadecyl-3, 3, 3′, 3′-tetramethylindodicarbocyanine, 4-chlorobenzenesulfonate salt (DiD) dye was purchased from Invitrogen/Thermo Fisher Scientific (Waltham, MA, USA). Cell culture media, including Dulbecco's modified Eagle's medium, fetal bovine serum, and penicillin/streptomycins were purchased from Hyclone (Logan, UT, USA). EGM-2-BulletKit medium was purchased from Lonza (Walkersville, MD, USA). ThinCerts inserts were obtained from Greiner Bio-One International (Frickenhausen, Germany). AccuPrep® PCR Purification Kit was purchased from Bioneer (Daejeon, Korea). Anti-human CXCR4 antibody, VEGF, and VEGF Quantikine ELISA kit was obtained from R&D Systems (Minneapolis, MN, USA). Anti- CD44, -CD90, -CD105, -CD34, -CD45, and -CD91 antibodies as well as APC-, PE-, FITC-, and PerCP-conjugated IgG isotype controls were purchased from Biolegend (San Diego, CA, USA). Cy3-conjugated anti-mouse IgG secondary antibody was obtained from ABM (Richmond, BC, Canada). Horseradish peroxidase–conjugated anti-mouse IgG secondary antibody was obtained from Santa Cruz Biotechnology (Dallas, TX, USA). Cell Counting Kit-8 was purchased from Dojindo Molecular Technologies, Inc. (Rockville, MD, USA). An anti-vascular endothelial (VE)-cadherin antibody was purchased from Abcam (Cambridge, UK). C57BL/6 mice (10-week-old, weighing 22–24 g) were purchased from Orient Bio Inc. (Seongnam, Korea). Sterile 0.45 μm Millex-GP syringe filters and Amicon Ultra centrifugal filter units were purchased from EMD Millipore (Billerica, MA, USA). All other chemicals (unless otherwise specified) were purchased from Sigma–Aldrich.

3. Methods

3.1. Isolation and characterization of hASC

hASCs were isolated from the infrapatellar fat pad, obtained from informed and consenting patients during knee replacement surgery. All experimental protocols were carried out in accordance with the approved guidelines of the ethical committee of CHA University. hASCs were isolated as previously described [21]. The isolated hASCs were cultured in Dulbecco's modified Eagle's medium supplemented with 10% (v/v) fetal bovine serum and 1% (v/v) penicillin/streptomycin at 37 °C in humidified air containing 5% CO_2. To validate their lineage integrity, the hASCs were analyzed by flow cytometry for positive MSC markers (CD44, CD90 and CD105) and the absence of negative surface markers (CD34, CD45 and CD91). Briefly, APC anti-human CD90, PE anti-human CD105, FITC anti-human CD44, PerCP anti-human CD34, FITC anti-human CD45 and FITC anti-human CD91 antibodies (1:100 dilution) were used for flow cytometry analysis. Positive populations of APC-, PE-, FITC- or PerCP-conjugated antibody-treated hASCs were normalized by APC-, PE-, FITC-, or PerCP-conjugated IgG isotypes treated hASCs, respectively.

3.2. Bioengineering of hASCs to express CXCR4

CXCR4 was PCR-amplified from human mRNA using sense primer 5′-TGGAGGGGATCAGTATATACCAC-3′ and antisense primer 5′-TTAG CTGGAGTGAAAACTTGAAGA-3´. PCR products were purified using the AccuPrep® PCR Purification Kit and cloned into the pTOP TA V2 vector (Enzynomics, Daejeon, Korea). To generate vector pMXs-*CXCR4*, the constructs were subcloned into the *Eco*RI site of vector pMXs (Cell Biolabs, San Diego, CA, USA). The expression vectors were purified using a NucleoSpin® Plasmid EasyPure kit (MACHEREY-NAGEL, Düren, Germany), and the insert was confirmed by sequencing. The GP2-293 retroviral packaging cell line was used to generate retrovirus. Briefly, GP2-293 cells, grown to 70% confluence in 100-mm dishes were transfected with 5 μg pMXs-*CXCR4* and 3 μg pMXs-VSV-g using the Convoy™ transfection reagent (ACTGene, Piscataway, NJ, USA). After 48 h of incubation, the retrovirus-containing supernatant was collected in conical tubes and centrifuged at 1000 rpm for 5 min to remove cell debris. Subsequently, the supernatant was filtered using a Millex-HV 0.45-μm filter and ultracentrifuged at 22,000 rpm for 2 h. The pellet containing virus aggregates was resuspended in 10 ml of fresh growth medium, supplemented with 8 ng/ml Polybrene, and then incubated with hASCs for 24 h.

3.3. Flow cytometry

Membrane expression of CXCR4 on hASCs was confirmed by flow cytometry. Retrovirally-transduced hASCs overexpressing CXCR4 were detached from 100-mm culture dishes using trypsin-EDTA, centrifuged at 1000 rpm for 5 min, and washed with phosphate-buffered saline (PBS). The cell pellet was resuspended and incubated at 4 °C for 1 h with anti-human CXCR4 antibody in PBS containing 1% BSA. Subsequently, the cells were washed three times in PBS, with centrifugation at 1000 rpm for 5 min. The pellet was resuspended with Cy3-conjugated secondary antibody in PBS containing 1% BSA, incubated at 4 °C for 30 min, and washed three times with PBS. hASCs labeled with Cy3-conjugated IgG isotypes were used as a negative control. The fluorescence intensity on the membranes of CXCR4-overexpressing hASCs was measured on an Accuri C6 (BD, MI) flow cytometer.

3.4. Western blotting

Protein levels in hASCs overexpressing CXCR4 were measured by western blotting. Cells were washed once with PBS, collected in 200 μl of radioimmunoprecipitation assay lysis buffer (RIPA) at 4 °C, and centrifuged at 13,000 rpm for 20 min at 4 °C. The supernatant was collected in 1.5-ml tubes, and protein concentrations were determined using a bicinchoninic acid (BCA) assay kit (Life Technologies, Rockford, IL, USA). Subsequently, samples containing 20 μg of total protein were separated by sodium dodecyl sulphate-polyacrylamide gel electrophoresis (SDS-PAGE), and then transferred to polyvinylidene fluoride (PVDF) membranes. The membranes were blocked with 5% skim milk in Tris-buffered saline containing 0.1% Tween-20 (TBS-T) for 30 min, washed three times with TBS-T, and incubated overnight at 4 °C with the primary antibody (1:1000 dilution) in TBS-T containing 5% BSA. Subsequently, the membranes were washed three times with TBS-T and incubated with secondary antibody (1:2000 dilution) in 5% skim milk in TBS-T at room temperature for 1 h. After three times washing with TBS-T, the signal was developed using the Amersham ECL Select Western Blotting Detection Reagent (GE Healthcare Life Sciences, Little Chalfont, UK) on a ChemiDoc™ XRS + System (Bio-Rad, Hercules, CA, USA).

3.5. Preparation of bioengineered stem cell membrane-coated nanocarriers (BSMNCs)

Bioengineered hASC-CXCR4 or non-engineered hASCs membrane-derived vesicles were prepared by hypotonic cell lysis as previously reported [22]. hASCs were washed with PBS and suspended in hypotonic buffer (Tris-magnesium buffer: 0.01 M Tris, and 0.001 M $MgCl_2$). The washed hASCs were homogenized at 22,000 rpm for 1 min on IKA T10 basic homogenizer, and then purified by centrifugation (6000 × g for 15 min). VEGF-poly (lactic-*co*-glycolic acid) (PLGA) nanocarriers (PNCs) were prepared by a modified double-emulsion solvent-evaporation method. Briefly, 100 μl of VEGF in PBS was emulsified with 2% (w/v) PLGA in dichloromethane under sonication. The resulting water-in-oil emulsion was then re-emulsified with water. The organic solvent was completely evaporated, and VEGF-PNCs or plain PNCs were collected by ultracentrifugation (60,000 × g in a Beckman Coulter Optima L-90K). For the preparation of Stem cell membrane coated nanocarrier (SMNCs), Bioengineered stem cell membrane-functionalized nanocarriers (BSMNCs), we used a simple sonication method reported previously [23]. Briefly, stem cell derived Nano ghost was mixed with PNCs. To a chive efficient coating, the mixture of PNCs and stem cell derived membrane material at a polymer to membrane protein weight ratio of 2:1 was then sonicated using an ultrasonic cleaner for 2–3 min. Finally, the excess of stem cell derived membrane materials were washed by ultracentrifugation process as mention early.

Encapsulation efficiency was calculated based on the amount of free VEGF in the supernatant. For VEGF release studies, 8 mg of PNC or VEGF-SMNC was dispersed in 1 ml of PBS and placed in a shaker incubator at room temperature. At specific time points, 400 μl of supernatant was aspirated and stored at −80 °C, and the same amount of PBS was added to the solution to keep volume constant. The quantity of released VEGF level was measured by ELISA.

For confocal microscopy, 2 μg of DiD dye was added to the organic solution prior to PNCs core synthesis. Similarly, to elucidate the core–shell structure of SMNCs, NBD-PC was incorporated into hASC membrane-derived vesicles, and the vesicles were then fused with DiD-loaded PNC cores. For *in vivo* studies, Cy5.5 was conjugated to the PLGA polymer as reported earlier method with modification [24]. Briefly, 24 mg of carboxyl-modified Cy5.5 in 1 ml dichloromethane (DCM) was mixed with 8.8 mg *N*,*N*-dicyclohexylcarbodiimide for 5 min. Then, 26 ml of dichloromethane containing 5.2 mg of 4-dimethylaminopyridine and 1.28 g of PLGA was added to the above mixture and incubated in the dark under gentle stirring. After 16 h, the reaction mixture was dried by rotary evaporation at room temperature, dissolved in 20 ml of acetonitrile, and transferred to two 50-ml conical tubes. To purify the product, 40 ml of methanol cooled in a dry-ice bath was added to each conical tube and centrifuged at 6000 × g for 15 min. The supernatant was discarded, and the washing procedure was repeated twice.

3.6. Physiochemical characterization

Mean particle diameter (Z-average), size distribution (PDI), and zeta potential (surface charge) of SMNCs and PNCs were determined by dynamic light scattering (DLS) using a Zetasizer Nano ZS system (Malvern Instruments Ltd., Worcestershire, UK). Shape and surface morphology were confirmed by energy-filtered transmission electron microscopy (EFTEM) and confocal microscopy (TCS SP5 II, Leica, Heidelberg, Germany). Additionally the presence of CXCR4 on BSMNCs were confirmed by Immunostaining followed by EFTEM [22]. Briefly, 20 μl of SMNCs or PNCs suspension (0.5 mg/ml) was deposited on a 200-mesh carbon-coated copper grid. Samples were blotted away after 30 min. Then the SMHNPs were rinsed with anti CXCR4 antibody. After 25 s of treatment, the unbound antibodies were washed. Finally, the anti-mouse IgG –gold antibody (Sigma-Aldrich) was added to the droplet and then washed with 5 drops of distilled water. Then, SMHNPs particle treated grid was stained with 1% uranyl acetate and visualized using EFTEM (Carl Zeiss LIBRA 120).

3.7. Phagocytosis assay

The phagocytic uptake of SMNCs, BSMNCs and PNCs was studied using murine J774 macrophages and human THP-1 monocyte cells. Briefly, J774 and THP-1 cells were cultured in DMEM media supplemented with 10% FBS and seeded in 12-well plates at a density of 10^5 cells/well (BD Biosciences). Prior to the experiment, the cells were washed with PBS, immersed in fresh medium, and incubated for 2 h with 30 μg/ml of each of the experimental NCs. Subsequently, the cells were washed with PBS and collected for flow cytometry analysis on a C6 Accuri™ system (BD Biosciences, MI). NP uptake was calculated as described previously [25].

3.8. Cytotoxicity assay

The cytotoxicity of SMNCs and PNCs on J774.1 and THP-1 cells was evaluated using the Cell Counting Kit-8 (CCK-8) assay. Cells were seeded in 24-well plates at a density of 6×10^4 cells/well. After incubation for 24 h, the medium was exchanged with 0.5 ml of culture medium containing of SMNCs or PNCs. Untreated cells were used as a control. After incubation for 48 h, the culture medium was replaced with 0.5 ml of CCK-8 reagent containing DMEM medium (1:10 dilution) and incubated for 1 h at 37 °C. Absorbance at 450 nm was measured in a Cytation 3 multi-mode microplate reader (BioTek Instruments, Winooski, VT, USA). Cell viability was expressed as a percentage relative to control (untreated) cells.

3.9. In vitro transendothelial penetration

Transwell experiments were performed as described previously [26]. Briefly, human umbilical vein endothelial cells (HUVECs) were obtained from the American Type Culture Collection (ATCC; PCS-100–013; Manassas, VA, USA) and processed according to the instructions of the provider. Cells were cultured and expanded using the EGM-2-BulletKit medium. During HUVEC expansion, 2 ng/ml VEGF and 2% gentamycin (PAN Biotech, Aidenbach, Germany) were added to the medium. After harvest, the cells were seeded on ThinCerts inserts. Before seeding, the membranes of the inserts were coated with 50 μg/ml fibronectin from human plasma (F2006, Sigma–Aldrich) for 1 h. TNF-α (0.1 μg/ml) was used to create an inflammatory state. Subsequently, SMNCs or PNCs were added to the Transwell chamber. After incubation

for 3 h, the medium was collected from each chamber. The lower chambers were washed with PBS and scraped twice to recover all particles. Filters bearing adhering cells were rinsed twice with PBS. The collected particles underwent nanoparticle tracking analysis (NTA; Nano Sight, Amesbury, UK). Samples were injected into a sample chamber with sterile syringes (Discardit II, Becton Dickinson, Franklin Lakes, NJ, USA) until the liquid reached the tip of the nozzle. All measurements were performed three times at room temperature. The NTA 2.3 software was used to analyze the results, and each sample was measured for 40 s with manual shutter and gain adjustments. The mean size and standard deviation (SD) values obtained by the NTA software correspond to the arithmetic values calculated from the sizes of all particles analyzed by the software. The number of filtered SMNCs was adjusted relative to the cell-free control to correct for particle entrapment in the filter itself.

3.10. Immunofluorescence staining

HUVECs were fixed with 4% paraformaldehyde, permeabilized with 0.1% Triton X-100, incubated with PBS containing 1% BSA, and then immunostained with antibodies against vascular endothelial (VE)–cadherin (1:200 dilution) for 40 min at room temperature. Cultures incubated with Alexa-488-conjugated goat IgG served as negative immunofluorescence controls. After washing, Alexa-488–conjugated donkey anti-goat secondary antibody (Invitrogen, CA, USA) was added for 40 min in the dark at room temperature.

3.11. Confocal microscopy

HUVECs were seeded at a density of 8×10^4 cells/filter on ThinCerts inserts coated with fibronectin and incubated for 3 h with SMNCs and PNCs containing an appropriate fluorophore. Subsequently, the cells were fixed and stained for actin as described by Parodi et al. [26]. Images were acquired with a confocal microscope (TCS SP5 II, Leica, Heidelberg, Germany) equipped with a 63 × oil-immersion objective and running the Leica LAS AF Ver 2.6 software (Fuji photo film. Tokyo, Japan).

3.12. Induction of hindlimb ischemia in a mouse model

All animal procedures were performed in accordance with a protocol approved by the institutional Animal Care and Use Committee (IACUC) of CHA University (IACUC160052). A total of eight female C57BL/6 mice (10-week-old, weighing 22–24 g) were raised at 55–65% humidity and controlled temperature of 24 ± 3 °C, with a light/dark cycle of 12 h. Mice had free access to food and tap water *ad libitum*. All animals were anaesthetized with a mixture of tiletamine hypochloride/zolazepam hypochloride (Zoletil, 50 mg/kg, Virbac Laboratories, France) and xylazine (Rompun, 10 mg/kg, Bayer, Korea), in saline. The femoral artery was ligated at two sites with a 6-0 silk suture. The femoral artery was excised from the distal to the external iliac artery and proximal to the popliteal arteries. After 3 days of induction, the tiptoes turned black, indicative of severe hindlimb ischemia. Thereafter, 150 μl of PBS containing SMNCs or BSMNCs loaded with VEGF (0.1 μg/mg polymer) was retro-orbitally injected.

3.13. Fluorescence imaging analysis in ischemic muscles

SMNCs and PNCs encapsulating the near-infrared fluorescent (NIF) dye (Cy-5.5) were injected retro-orbitally (150 μl of NPs) in ischemic mice 3 days after surgery. Subsequently, the animals were scanned using a Pearl Impulse small animal imager (Li-Cor, Bioscience, NE) to monitor fluorescence signals in ischemic muscle 1, 3, 7 and 14 days post-injection. The Pearl Impulse imager can use two excitation laser lines for image acquisition, at wavelengths of 700 or 800 nm; in this study, only the 700 nm excitation line was used. Each image was acquired at a resolution of 85 μm. The images were analyzed to quantify blood flow in the region of interest and mean values of fluorescence intensity. The mice were anaesthetized with 2% isoflurane during scanning and sacrificed at the end of experiment.

3.14. Assessment of limb salvage

Tissue necrosis of the ischemic hindlimb was evaluated via both gross observation of the hindlimb status and blood reperfusion. Gross examination was performed 0, 1, 3, 7, 14 and 28 days after retro-orbital (RO) injection, and scoring of hindlimb salvage was performed at the final time point. Ischemic hindlimb severity was graded as: 1) limb loss, 2) limb salvage (10%) and 3) limb salvage (50%).

3.15. Histological analysis

Tissue samples of ischemic muscles were separated and fixed in 4% paraformaldehyde for 24 h. Tissue blocks were sectioned at a thickness of 4 μm. Sections were stained with hematoxylin and eosin for morphological analysis, and with Masson's trichrome to evaluate fibrosis of the ischemic muscle.

3.16. Laser Doppler imaging analysis

Laser Doppler imaging analysis was performed with a laser Doppler perfusion imager (LDPI, Moor Instruments, Devon, UK). Blood flow to the right and left hindlimbs was monitored for serial non-invasive physiological evaluation of neovascularization 0, 1, 3, 7, 14, and 28 days after treatment. Mice were placed on a warming plate at 37 °C before scanning was initiated. The limb perfusion ratio was calculated from the ratio of ischemic to non-ischemic hindlimbs.

3.17. Statistical analysis

The experiments for each condition were performed in triplicate. Data from replicate experiments were pooled, and standard errors of the mean (SEM) were calculated. Analysis of variance (ANOVA) was used to evaluate statistical significance, and the Bonferroni post-test was used for comparisons between groups. Differences were considered significant at $P < 0.05$. The GraphPad Prism software (version 5.02) was used to perform statistical tests.

4. Results

4.1. Preparation and characterization of SMNCs

We used hASCs as a cell source for the preparation of stem cell membrane-coated nanocarriers. To validate lineage integrity, each batch of hASCs was analyzed by flow cytometry for the presence (CD44, CD90, and CD105) and absence (CD31) of MSC markers [27]. As shown in Fig. S1, the cells expressed all three positive hASC markers while showing negative for CD31. For the preparation of SMNCs (Fig. 1A), nanoghosts derived from non-engineered was prepared as per the protocols described previously [25,28]. The process of preparation of hASC membrane-derived vesicles was monitored microscopically (Fig. 1B and C). It is anticipated that the preparation process may allow the hASCs derived vesicles maintain the structural integrity of transmembrane receptors by keeping them in their physiological membrane [29]. Subsequently, VEGF-PNC cores were prepared and fused with hASC membranes by previously reported sonication method [23]. It was shown that the surface glycan's on cell membranes and the substrate properties many play a crucial role in driving and directing the cell membrane–particle assembly [30]. To achieve efficient coating, the mixture of PNCs and stem cell derived membrane material at a polymer to membrane protein weight ratio of 2:1 was then sonicated using an ultrasonic cleaner for 2–3 min. Finally, the excess of stem cell derived

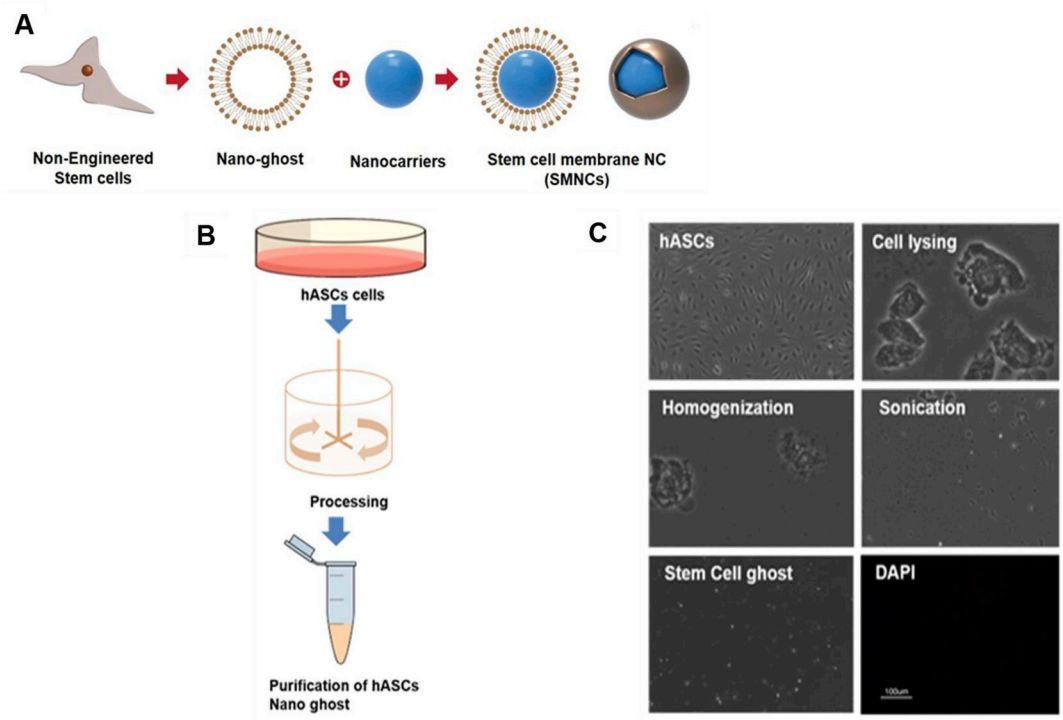

Fig. 1. Preparation of stem cell membrane-nanocarrier (SMNCs). (A) Schematic showing the concept and preparation of stem cell membrane nanocarriers (SMNCs), (B) Schematic diagram details the preparation of hASC membrane-derived nanoghosts. (C) Microscopic observation of membrane separation from culture-expanded hASCs. Nuclear staining (DAPI) was used to differentiate between cell debris and hASC-derived nanoghosts. (Scale bars, 100 nm).

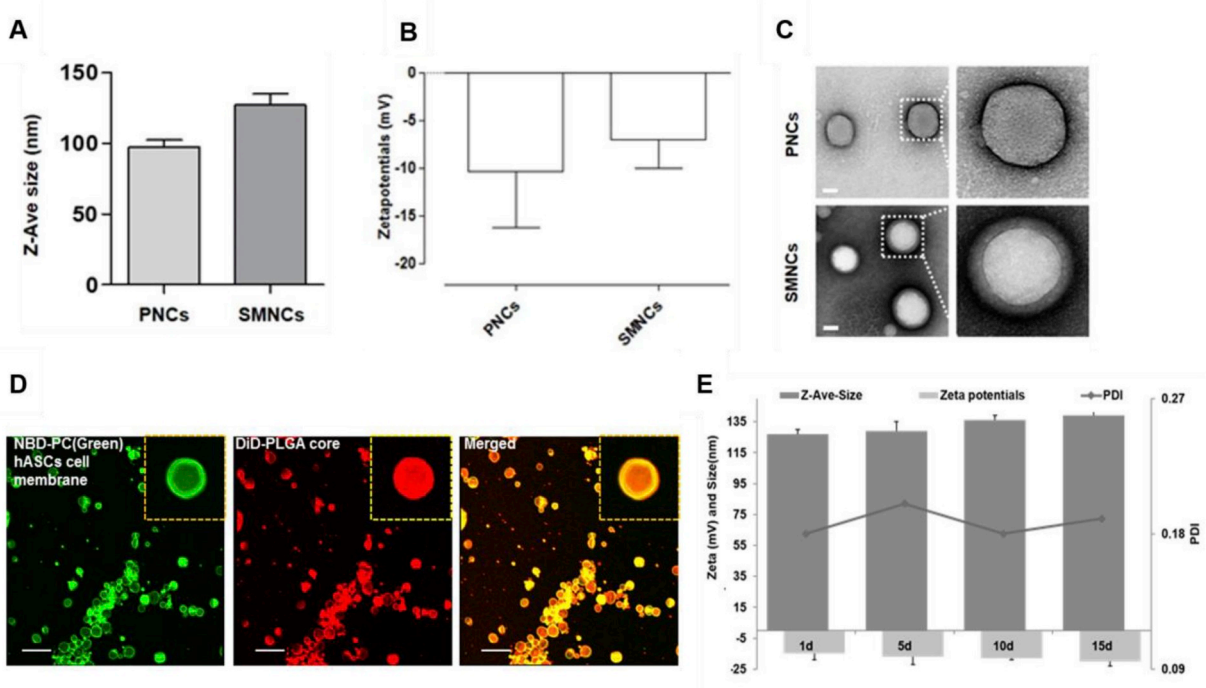

Fig. 2. Characterization of stem cell membrane-nanocarrier (SMNCs). (A) Average hydrodynamic sizes of PLGA nanocarriers (PNCs) and SMNCs, (B) Zeta potentials of non-functionalized PNCs and SMNCs, and (C) Transmission electron microscopy images of non-functionalized PNCs and SMNCs. SMNCs were negatively stained with uranyl acetate (Scale bars, 50 nm). (C) CLSM images of PNCs functionalized with stem cell membranes. Confocal laser scanning micrographs showing the core–shell structure of SMNCs. NBD-PC (green) was incorporated into hASC membrane-derived vesicles, and the vesicles were then fused with DiD(red)-loaded PNC cores. (Scale bar, 1 μm). (E) Size, charge, and polydispersity index of SMNCs monitored by DLS. (For interpretation of the references to colour in this figure legend, the reader is referred to the Web version of this article.)

membrane materials were washed by ultracentrifugation process as mention early. Functionalization of PNCs with engineered or non-engineered hASC membranes resulted in an increase in particle size, from 97 ± 2 nm (PNCs) to 127 ± 6 nm (SMNCs) (Fig. 2A and Fig. S3), and in zeta potential from −29.2 ± 1.6 mV (PNCs) to −15 ± 1.3 mV (SMNCs) (Fig. 2B). EFTEM confirmed the formation of hybrid Nano

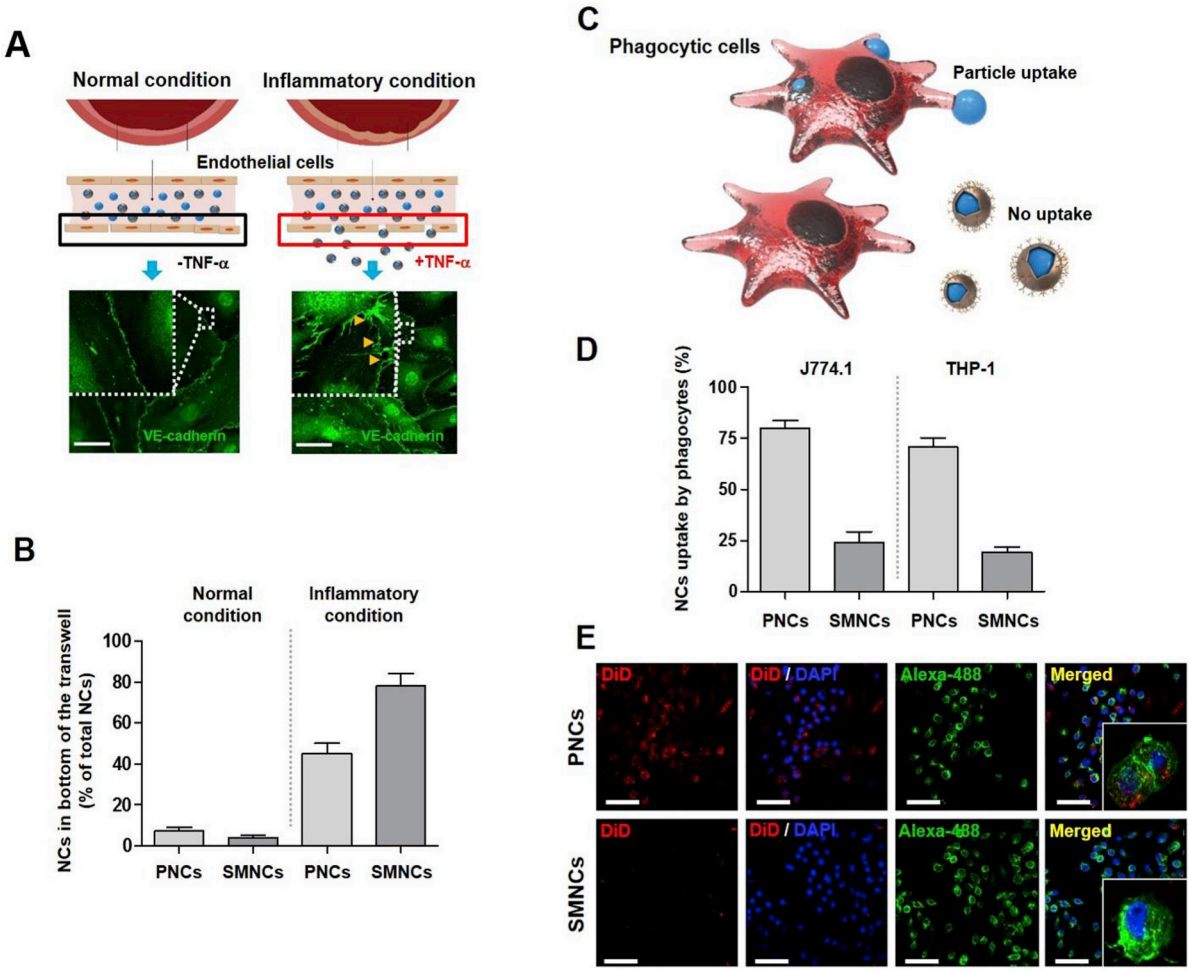

Fig. 3. Improved transendothelial penetration and reduced phagocyte uptake of SMNCs. (A) Schematic outline and fluorescence images of *in vitro* transendothelial penetration following stimulation with the inflammatory mediator, TNF-α. VE–cadherin is shown in green (Scale bars, 25 μm). (B) The therapeutic potential of stem cell membrane functionalization assessed using an *in vitro* transwell model comprising healthy endothelial monolayer versus inflamed (TNF-α -treated) endothelial monolayers. (C) Schematic diagram of the internalization of PNCs and SMNCs by phagocytic cells. (D) Flow cytometry analysis of internalization of PNCs and SMNCs by J774 and THP macrophage cells. (E) Confocal microscopic images showing internalization of PNCs and SMNCs by J774 cells. Fluorescent PNCs and SMNCs were prepared by incorporation of DiD (red). Actin and the nucleus were stained with Alexa Fluor 488 (green) and DAPI (blue), respectively (Scale bars, 50 μm). (For interpretation of the references to colour in this figure legend, the reader is referred to the Web version of this article.)

sphere consisting of a PLGA core covered by a thin lipid layer (Fig.2C and Fig.S2) [19]. The core–shell hybrid structure of SMNCs was confirmed using a dual-fluorophore labeling technique: 1,1′-Dioctadecyl-3,3,3′,3′-Tetramethylindodicarbocyanine, 4-Chlorobenzenesulfonate (DiD) dye was loaded into the PLGA core, and the fluorescent lipid 1-oleoyl-2-[12-[(7-nitro-2-1,3-benzoxadiazol-4-yl) amino] dodecanoyl]-sn-glycero-3-phosphocholine] NBD-PC was incorporated into the hASC membrane-derived vesicles prior to hASC vesicle–PLGA fusion. The dual-fluorophore-labeled SMNCs visualized by confocal laser scanning microscopy confirmed the presence of DiD (red) and NBD-PC (green) signals perfectly corresponding to the PNC core and membrane portions of the SMNCs, respectively (Fig. 2D). In addition, the merged image clearly demonstrated the successful fabrication of SMNCs with a core–shell structure [31]. Next, we assessed the stability of SMNCs by monitoring changes in their size and distribution by DLS (Fig. 2E) [19,32]. The particle size increased slightly, from 127 nm to 139 nm, whereas the polydispersity index (PDI) did not show much change. This change in size and zeta potential were presumably caused by the fusion of a small amount of excess vesicles in the particle suspension.

4.2. Enhanced transendothelial penetration of SMNCs

Inflammation plays a pivotal role in endothelial dysfunction. Pro-inflammatory cytokines such as tumor necrosis factor (TNF-α) contribute to endothelial cell activation by promoting adhesion and migration of stem cells across the inflamed endothelium [24]. Hence, we hypothesized that functionalization of PNCs with stem cell membranes could enable the particles to readily penetrate the endothelium under inflammatory conditions [33]. To investigate the mechanisms underlying this particular behavior of SMNCs, we established a Transwell-based *in vitro* model system of endothelial cells (ECs) activated by TNF-α, as shown in Fig.S4 (A). Indeed, TNF-α activation induced disruption of intercellular junction structures between ECs, as demonstrated by the patchy expression of VE-cadherin (Fig. 3A). Under normal condition, a few PNCs crossed the EC barrier, whereas under inflammatory condition, considerable number of both PNCs and SMNCs crossed the barrier (Fig. 3B). Interestingly, under inflammatory conditions, the number of SMNCs that penetrated the EC barrier was much higher than the number of PNCs [33]. Furthermore, cconfocal microscopy of HUVEC treated with PNCs or SMNCs (Red and green merged) for 3 h showed

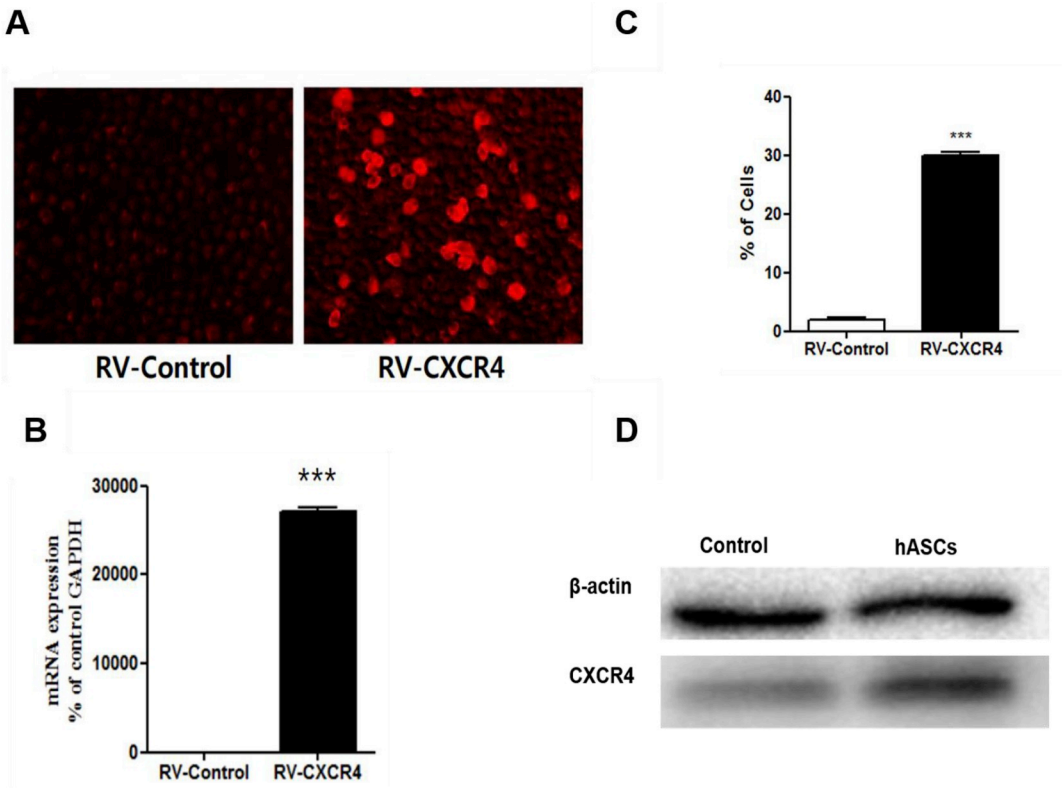

Fig. 4. Validation of CXCR4 expression on hASCs. (A) Immunofluorescence analysis of CXCR4 expression on membranes of hASCs using an anti-CXCR4 primary antibody and a Cy3-conjugated anti-mouse IgG secondary antibody. (B) Quantification of CXCR4-positive hASCs by flow cytometry. (C) Quantification of CXCR4 mRNA levels by quantitative PCR. (D) Western blot analysis of CXCR4 (40 kDa) and β-actin (42 kDa) expression in hASCs.

reorganization of cytoskeletons (Fig.S4). The observed pattern was consistent with the early reports by Parodi et al. [26].

4.3. Reduced in vitro phagocyte uptake of SMNCs

Systemic administration of nanomedicine often fails to translate to clinical benefit due to rapid clearance of the therapeutic agents from the circulation by macrophages [13,34]. Accordingly, preventing recognition and delaying the uptake of PNCs by phagocytic cells is a promising strategy for improving the efficacy of such therapies [13,14,25]. MSCs, including ASCs, have hypoimmunogenic and strong immune modulatory properties [35]. The interaction between MSCs and immune cells is a key factor in the immunomodulatory effects of MSCs [36,37]. Hence, we hypothesized that stem cell membrane functionalization of PNCs could reduce phagocytic uptake (Fig. 3C). To verify our hypothesis, we treated J774 and THP cells with DiD-labeled SMNCs and PNCs, and then performed flow cytometry analysis. Fig. 3D shows that the stem cell membrane functionalization of PNCs significantly decreased the uptake by J774 and THP cells: 84% and 76% of PNCs were internalized into J774 and THP cells respectively, which was reduced to 29% and 24% in SMNCs. Fig. 2E shows a fluorescence image of J774 cells cultured with SMNCs and PNCs. Confocal microscopy revealed that both SMNCs and PNCs were phagocytosed into the cytoplasm, and that J774 cells internalized more PNCs than SMNCs, consistent with the previous results. Overall, our studies showed that the presence of stem cell membrane-derived lipids on PNCs inhibited particle uptake by macrophages. Macrophages are a type of white blood cell that sense and internalize foreign materials, including nanoparticles, via a process called phagocytosis. Stem cell–mimetic functionalization of the PNC surface could disguise PNCs as stem cells, preventing recognition by macrophages and thereby decreasing SMNC uptake. Notably, the functionalization of the PNC surface with stem cell membranes did not affect the viability of murine or human macrophages (Fig.S5).

4.4. Preparation of BSMNCs from CXCR4 expression engineered hASCs

Our main strategy was to compare non-engineered SMNCs and engineered BSMNCs as schematically illustrated in Figs. 1A and 5A. To generate CXCR4-expressing hASCs, a retroviral vector system encoding *CXCR4* was used. *CXCR4* expression was detected by fluorescence microscopy (Fig. 4A), confirming that the retroviral particles expressing *CXCR4* were correctly packaged, and CXCR4 expression at the mRNA level was verified by quantitative reverse transcription polymerase chain reaction (qRT-PCR) (Fig. 4B). The number of cells expressing CXCR4 protein was significantly elevated following retroviral transduction (30 ± 2.0%) in comparison with controls (4.4 ± 0.8%; $p < 0.05$) (Fig. 4C). This result was further confirmed by western blotting, which demonstrated higher expression of CXCR4 protein in hASCs after transduction with RV-CXCR4 (Fig. 4D). BSMNCs was also prepared from the nanoghosts derived from bioengineered hASCs (CXCR4-hASCs) by the same protocols as described previously [25,28].

4.5. Biodistribution and time-dependent targeting capability of BSMNCs

To improve the targeting ability of SMNCs, we prepared membranes from hASCs bioengineered to overexpress CXCR4 receptor. Bioengineered membrane coated SMNCs (BSMNCs) were prepared from nanoghosts derived from CXCR4-hASCs (Fig. 5A). The western blotting and EFTEM-immunostaining (Fig. 5B) confirmed the successful transfer of the engineered stem cell membranes onto the PNCs and validated the orientation of CXCR4 on the surface of BSMNCs [13]. These results demonstrate that this fabrication technique is able to induce the expression of CXCR4 proteins on reconstructed hASC membranes transferred onto the surface of BSMNCs. The time-dependent targeting efficiency of SMNCs and BMSNCs was investigated in a murine model of

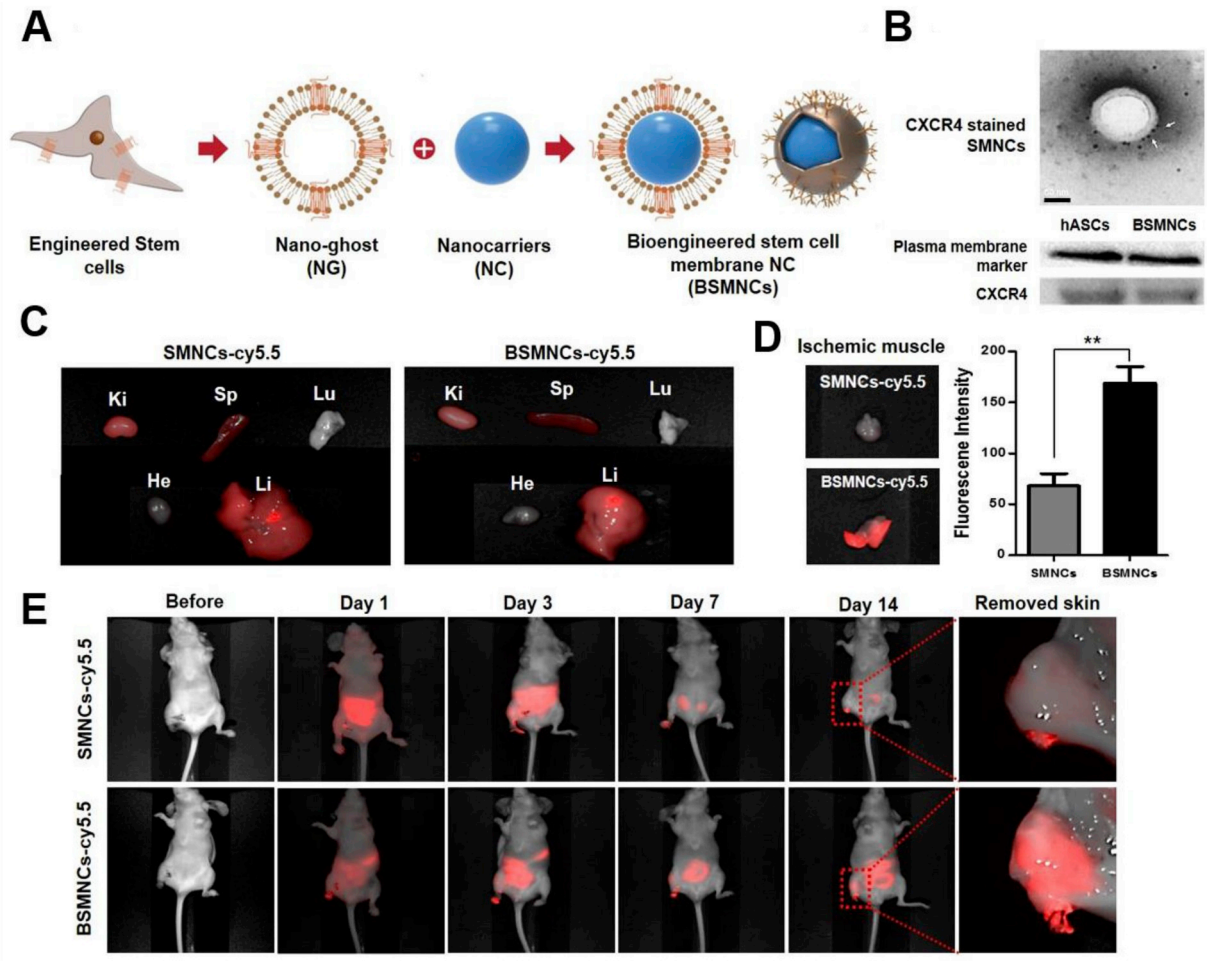

Fig. 5. Characterization of bioengineered stem cell membrane nanocarriers (BSMNCs) and time-dependent *in vivo* distribution of BSMNCs and SMNCs in murine hindlimb ischemia. (A) Schematic showing the concept and preparation of bioengineered stem cell membrane-nanocarriers (BSMNCs). (B) TEM images of immunostaining micrograph showing CXCR4 orientation on SMNCs stained with CXCR4 antibodies and a secondary anti-CXCR4 (upper) (Scale bars, 50 nm). Western blot analysis showing translocation of CXCR4 from hASCs to the surface of BSMNCs (lower). (C) Biodistribution of BSMNCs and SMNCs after 14 days. Ki: kidney, Sp: spleen, Lu: lung, He: heart, Li: liver. (D) Quantitative image of *ex vivo* fluorescence intensity of ischemic induced muscles after IV injection of SMNCs or BSMNCs. (E) *In vivo* images of mice retro-orbitally injected with SMNC-Cy5 or BSMNC-Cy5 nanocarriers, before injection and 1, 3, 7 and 14 days after injection.

severe hindlimb ischemia that was induced 3 days after artery excision. In these experiments, Cy-5.5–labeled SMNCs and BMSNCs were administered intravenously. Fig. 5C–E shows the biodistribution of SMNCs and BMSNCs after a 14-day exposure. Cy-5.5 fluorescence signals were predominantly detected in the liver, kidney, and spleen, whereas no signal was detected in lung or heart tissues (Fig. 5C). *Ex vivo* fluorescence intensity quantitative analysis demonstrated the superior targeting ability of BSMNCs to ischemic muscle tissues compared to SMNCs (Fig. 5D). Whole-body fluorescence imaging revealed the time-dependent and tissue-specific BSMNC tropism towards ischemic tissues (Fig. 5E). Upon intravenous administration of Cy-5.5-labeled BSMNCs, the fluorescence signal from BSMNCs in the ischemic tissues remained stronger for over 14 days, whereas the signal raised from SMNCs decreased rapidly within 3 days. These studies demonstrated the potential use of BSMNCs for targeted therapeutic delivery to hindlimb ischemic tissues.

4.6. Enhanced blood reperfusion and improved limb salvage by BSMNCs

To evaluate the efficiency of VEGF mediated reperfusion that can be achieved by BSMNCs loaded with VEGF we first characterized PNCs loaded with VEGF. The *in vitro* VEGF release profile of VEGF-PNCs is shown in Fig.S6. VEGF release from PNCs exhibited a biphasic pattern with an initial burst followed by sustained release. The burst within 1 day resulted in release of more than 35% of the VEGF into the supernatant; nearly 70–80% of VEGF was released within 1 month. By contrast, hASC cell membrane functionalization of PNCs efficiently controlled the kinetics of VEGF release, with release of 15% and 55% by day 1 and day 30, respectively. These experimental results show that the surfaces of hASC membrane-functionalized PNCs can act as a diffusion barrier, which could slow down VEGF release in comparison PNCs without membrane [13].

We evaluated the therapeutic efficacy of SMNCs and BMSNCs loaded with VEGF by monitoring functional blood reperfusion and limb outcome [38,39]. A total of 150 μl of PBS containing SMNCs or BMSNCs loaded with VEGF (0.1 μg/mg polymer) was delivered into hindlimbs via RO injection at 3 days after artery excision. To investigate functional blood reperfusion, we performed laser Doppler imaging analysis. For serial non-invasive physiological evaluation of neovascularization, blood flow to the right and left hindlimbs was monitored at days 0, 1, 3, 7, 14 and 28 after treatment with VEGF-SMNCs or VEGF- BMSNCs. The ischemic status of the limb was confirmed at day 0 post-surgery. As illustrated in the laser Doppler images (Fig. 6A), the groups treated with BSMNCs exhibited significantly enhanced blood reperfusion at days 7, 14 and 28 than the SMNC-treated and control groups ($P < 0.01$ and $P < 0.001$ versus control and SMNCs, respectively). The relative ratio of limb perfusion (Fig. 6B) revealed significant improvement in blood reperfusion after day 3 in the BSMNC-treated group, whereas the

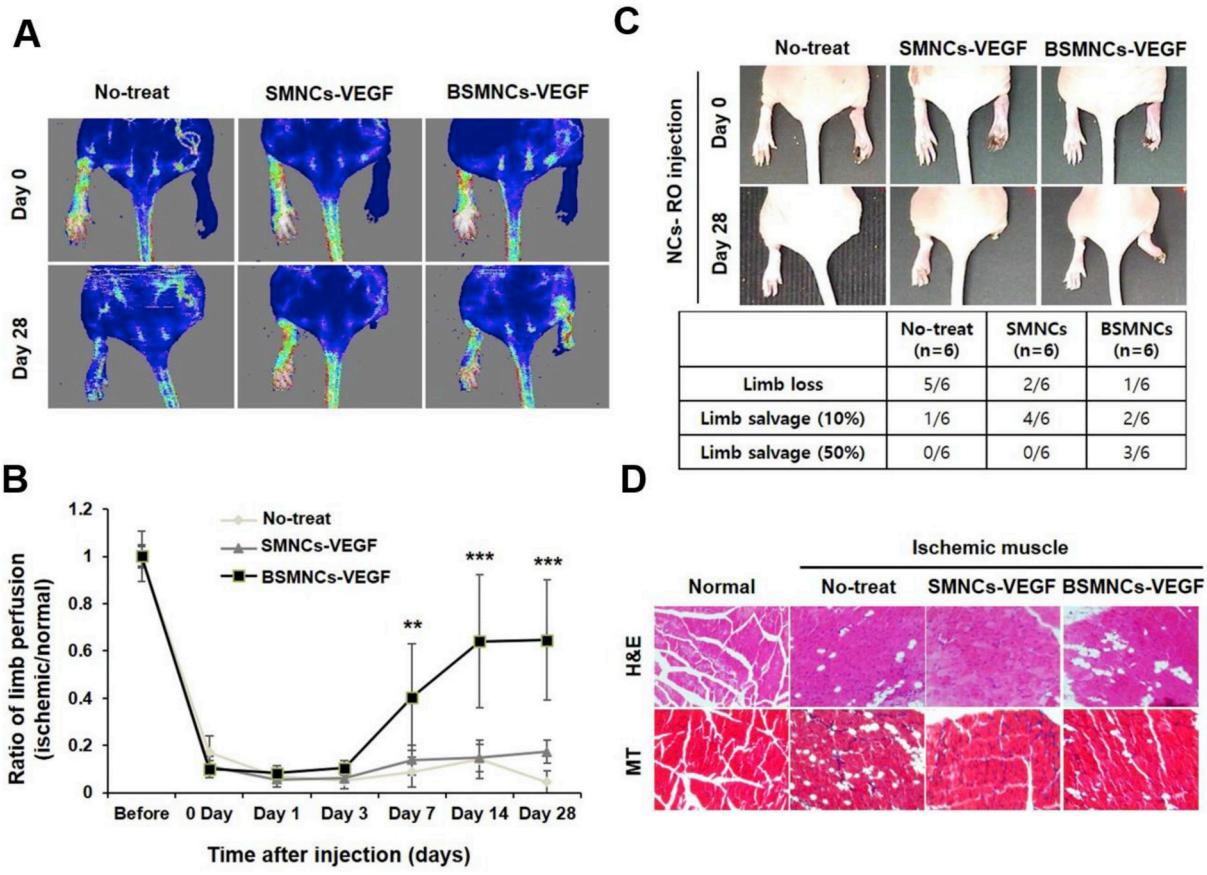

	No-treat (n=6)	SMNCs (n=6)	BSMNCs (n=6)
Limb loss	5/6	2/6	1/6
Limb salvage (10%)	1/6	4/6	2/6
Limb salvage (50%)	0/6	0/6	3/6

Fig. 6. Revascularization of ischemic limb and reduction of limb loss by SMNCs and VEGF-BSMNCs in a severe hindlimb ischemic mouse model. (A) Representative laser Doppler perfusion imaging of hindlimb ischemia treated with SMNCs or VEGF-BSMNCs at the indicated time points after injection. (B) Quantitative analysis of blood perfusion ratio (ischemic/normal) on days 1, 3, 7, 14 and 28, (**$P < 0.01$, ***$P < 0.001$ versus control and SMNCs). (C) Physiological status of ischemic hindlimb before and 28 days after VEGF-NC injection. (D) Histological analysis of ischemia induction. Samples were stained with Masson's trichrome.

SMNC-treated and control groups exhibited less or no therapeutic effect at day 3. The efficacy of BSMNCs and SMNCs for limb salvage was evaluated by assessing the physiological status of the ischemic hindlimbs 28 days after treatment with VEGF-SMNCs or VEGF- BMSNCs administered via RO injection. Tissue necrosis of the ischemic hindlimb was evaluated by both gross observation of hindlimb status and blood reperfusion at the final time point. The severity of hindlimb ischemia was categorized into three levels: limb loss, 10% limb salvage, and 50% limb salvage (Fig.S7). The results indicated improved limb recovery and superior therapeutic response in 50% of the tested animals (n = 6) in the BSMNC-treated group. The untreated group exhibited a higher percentage (83%) of limb loss, whereas treatment with SMNCs (33%) and BSMNCs (17%) efficiently prevented limb loss (Fig. 6C). The superior ischemic tissue-specific accumulation of BSMNCs led to stable blood reperfusion, thereby improving limb salvage while reducing limb loss in the animals tested. Furthermore, histological analysis of the ischemic tissue also demonstrated enhanced muscle fiber regeneration in the BSMNC-treated group (Fig. 6D). Overall, BSMNCs significantly improved therapeutic outcome in terms of limb recovery and significantly reduced limb loss in the animals tested.

5. Discussion

Peripheral vascular disease (PVD) causes significant morbidity and mortality in high-risk populations [40]. Numerous therapeutic strategies have been developed to promote vascular growth and regeneration, including gene therapy, growth factor delivery, and stem cell therapy [40]. Among these treatment strategies, engineered stem cell therapy has been extensively studied because of its unique ability to customize the properties of stem cells [5,41]. However, the potential of engineered stem cells for PVD treatment has not been realized, largely due to challenges related to safety, scalability and reproducibility. Alternatively, CMNCs have been developed to overcome the limitations of cell-based therapy [13,17].

In this study, both non-engineered SMNCs and engineered BSMNCs were prepared by general methods as described previously [13,42]. We found that bio-functionalization of nanocarriers with engineered stem cell membranes expressing CXCR4 exhibited improved tropism towards the ischemic tissue, leading to faster restoration of blood perfusion and rapid limb salvage even in a severe hindlimb ischemia model of PVD. By comparison, non-engineered SMNCs exhibited poor homing to the ischemic tissue, leading to poor blood perfusion and limb loss compared to CXCR-SMNCs. Histological analysis further confirmed that the presence of CXCR4 on BSMNCs accelerated the regeneration of new muscle fibers in ischemic tissues 28 days after BMSNC treatment. These findings also demonstrated that BMSNCs exert a beneficial effect on limb recovery in ischemic tissues *in vivo*. CXCR4–SDF interactions contributed to BSMNC-enhanced tropism towards ischemic tissue, which promoted an early angiogenic response and strong reperfusion action, resulting in improved limb healing. These findings were further supported by our *in vitro* data. Stem cell membrane functionalization of NCs considerably decreased their uptake by phagocytes and significantly promoted their penetration across inflamed endothelial barrier. By contrast, uncoated PNCs were efficiently taken-up by immune cells and exhibited a limited ability to penetrate across endothelial barriers. Collectively, our results provide proof of principle for a

versatile strategy for improving targeting of stem cell–nanoparticle hybrids through functionalization of polymeric NCs with membranes isolated from genetically-engineered hASCs expressing CXCR4. The advantages of stem cell membrane coating were demonstrated *in vitro* by phagocytosis and transwell assays.

In summary, BSMNCs enabled natural targeting to ischemic tissues, leading to rapid blood perfusion and limb salvage. Stem cell membrane coating of PNCs considerably decreased their uptake by immune cells and promoted their translocation across endothelial barriers. Furthermore, our approach could be generalized by engineering stem cells with different functional proteins of interest and/or adding a drug payload within the polymeric core. Thus, the BSMNCs described here have tremendous potential for use in therapies based on systemic delivery, and could be applied in a broad range of biomedical contexts. Moreover, given the benefits of scalable stem cell sources and the biodegradability of the polymeric core, our approach could be easily translated to the bedside.

Data availability

All the data needed to reproduce the work performed and evaluate the conclusions made are presented in the paper and/or the Supplemental Materials. Additional raw/processed data required to reproduce these findings cannot be shared at this time as the data also forms part of an ongoing study.

Sources of funding

This research was supported by the National Research Foundation of Korea, funded by the Ministry of Science, ICT and Future Planning, and the Korean Government (MSIP) (NRF-2016R1A2A1A05004987) and Creative Materials Discovery Program through the National Research Foundation of Korea (NRF) funded by Ministry of Science and ICT (NRF-2018M3D1A1058813).

Disclosures

None.

Appendix A. Supplementary data

Supplementary data related to this article can be found at https://doi.org/10.1016/j.biomaterials.2018.08.018.

References

[1] M.H. Shishehbor, C.J. White, B.H. Gray, M.T. Menard, R. Lookstein, K. Rosenfield, M.R. Jaff, Critical limb ischemia: an expert statement, J. Am. Coll. Cardiol. 68 (18) (2016) 2002–2015.
[2] N. Idei, J. Soga, T. Hata, Y. Fujii, N. Fujimura, S. Mikami, T. Maruhashi, K. Nishioka, T. Hidaka, Y. Kihara, Autologous bone-marrow mononuclear cell implantation reduces long-term major amputation risk in patients with critical limb IschemiaClinical perspective, Circ. Cardiovasc. Interv. 4 (1) (2011) 15–25.
[3] S.-H. Heo, Y.-S. Park, E.-S. Kang, K.-B. Park, Y.-S. Do, K.-S. Kang, D.-I. Kim, Early results of clinical application of autologous whole bone marrow stem cell transplantation for critical limb ischemia with Buerger's disease, Sci. Rep. 6 (2016).
[4] P.A. Tebebi, S.J. Kim, R.A. Williams, B. Milo, V. Frenkel, S.R. Burks, J.A. Frank, Improving the therapeutic efficacy of mesenchymal stromal cells to restore perfusion in critical limb ischemia through pulsed focused ultrasound, Sci. Rep. 7 (2017).
[5] B.H. Annex, Therapeutic angiogenesis for critical limb ischaemia, Nat. Rev. Cardiol. 10 (7) (2013) 387–396.
[6] C. Yellowley, CXCL12/CXCR4 signaling and other recruitment and homing pathways in fracture repair, BoneKEy Rep. 2 (3) (2013).
[7] Y.-W. Won, A.N. Patel, D.A. Bull, Cell surface engineering to enhance mesenchymal stem cell migration toward an SDF-1 gradient, Biomaterials 35 (21) (2014) 5627–5635.
[8] Z. Wang, Y. Wang, Z. Wang, J.S. Gutkind, Z. Wang, F. Wang, J. Lu, G. Niu, G. Teng, X. Chen, Engineered mesenchymal stem cells with enhanced tropism and paracrine secretion of cytokines and growth factors to treat traumatic brain injury, Stem Cell. 33 (2) (2015) 456–467.
[9] P.K. Nguyen, J. Riegler, J.C. Wu, Stem cell imaging: from bench to bedside, Cell stem cell 14 (4) (2014) 431–444.
[10] M.F. Kircher, S.S. Gambhir, J. Grimm, Noninvasive cell-tracking methods, Nat. Rev. Clin. Oncol. 8 (11) (2011) 677–688.
[11] Y.Y. Lipsitz, P. Bedford, A.H. Davies, N.E. Timmins, P.W. Zandstra, Achieving efficient manufacturing and quality assurance through synthetic cell therapy design, Cell Stem Cell 20 (1) (2017) 13–17.
[12] N. Trainor, A. Pietak, T. Smith, Rethinking clinical delivery of adult stem cell therapies, Nat. Biotechnol. 32 (8) (2014) 729.
[13] R.J. Bose, S.-H. Lee, H. Park, Biofunctionalized nanoparticles: an emerging drug delivery platform for various disease treatments, Drug Discov. Today 21 (8) (2016) 1303–1312.
[14] D. Dehaini, X. Wei, R.H. Fang, S. Masson, P. Angsantikul, B.T. Luk, Y. Zhang, M. Ying, Y. Jiang, A.V. Kroll, Erythrocyte–Platelet hybrid membrane coating for enhanced nanoparticle functionalization, Adv. Mater. 29 (16) (2017).
[15] R.J. Bose, R. Paulmurugan, J. Moon, S.H. Lee, H. Park, Cell membrane-coated nanocarriers: the emerging targeted delivery system for cancer theranostics, Drug Discov. Today 23 (4) (2018) 891–899.
[16] H. Zhou, Z. Fan, P.K. Lemons, H. Cheng, A facile approach to functionalize cell membrane-coated nanoparticles, Theranostics 6 (7) (2016) 1012.
[17] B.T. Luk, L. Zhang, Cell membrane-camouflaged nanoparticles for drug delivery, J. Contr. Release 220 (2015) 600–607.
[18] Y. Jin, J.S. Lee, S. Min, H.J. Park, T.J. Kang, S.W. Cho, Bioengineered extracellular membranous nanovesicles for efficient small-interfering RNA delivery: versatile platforms for stem cell engineering and in vivo delivery, Adv. Funct. Mater. 26 (32) (2016) 14.
[19] J. Tang, T. Su, K. Huang, P.-U. Dinh, Z. Wang, A. Vandergriff, M.T. Hensley, J. Cores, T. Allen, T. Li, E. Sproul, E. Mihalko, L.J. Lobo, L. Ruterbories, A. Lynch, A. Brown, T.G. Caranasos, D. Shen, G.A. Stouffer, Z. Gu, J. Zhang, K. Cheng, Targeted repair of heart injury by stem cells fused with platelet nanovesicles, Nat. Biomed. Eng. 2 (2018) 17–26.
[20] H.D. Theiss, M. Vallaster, C. Rischpler, L. Krieg, M.M. Zaruba, S. Brunner, Y. Vanchev, R. Fischer, M. Grobner, B. Huber, T. Wollenweber, G. Assmann, J. Mueller-Hoecker, M. Hacker, W.M. Franz, Dual stem cell therapy after myocardial infarction acts specifically by enhanced homing via the SDF-1/CXCR4 axis, Stem Cell Res. 7 (3) (2011) 244–255.
[21] C.A. Tannoury, H.S. An, Complications with the use of bone morphogenetic protein 2 (BMP-2) in spine surgery, Spine J. 14 (3) (2014) 552–559.
[22] C.-M.J. Hu, R.H. Fang, B.T. Luk, K.N. Chen, C. Carpenter, W. Gao, K. Zhang, L. Zhang, 'Marker-of-self'functionalization of nanoscale particles through a top-down cellular membrane coating approach, Nanoscale 5 (7) (2013) 2664–2668.
[23] D. Dehaini, X. Wei, R.H. Fang, S. Masson, P. Angsantikul, B.T. Luk, Y. Zhang, M. Ying, Y. Jiang, A.V. Kroll, Erythrocyte–platelet hybrid membrane coating for enhanced nanoparticle functionalization, Adv. Mater. 29 (16) (2017) 1606209.
[24] Y. Kim, M.E. Lobatto, T. Kawahara, B.L. Chung, A.J. Mieszawska, B.L. Sanchez-Gaytan, F. Fay, M.L. Senders, C. Calcagno, J. Becraft, Probing nanoparticle translocation across the permeable endothelium in experimental atherosclerosis, Proc. Natl. Acad. Sci. U. S. A. 111 (3) (2014) 1078–1083.
[25] C.-M.J. Hu, L. Zhang, S. Aryal, C. Cheung, R.H. Fang, L. Zhang, Erythrocyte membrane-camouflaged polymeric nanoparticles as a biomimetic delivery platform, Proc. Natl. Acad. Sci. U. S. A. 108 (27) (2011) 10980–10985.
[26] A. Parodi, N. Quattrocchi, A.L. Van De Ven, C. Chiappini, M. Evangelopoulos, J.O. Martinez, B.S. Brown, S.Z. Khaled, I.K. Yazdi, M.V. Enzo, Synthetic nanoparticles functionalized with biomimetic leukocyte membranes possess cell-like functions, Nat. Nanotechnol. 8 (1) (2013) 61–68.
[27] F. De Francesco, G. Ricci, F. D'Andrea, G.F. Nicoletti, G.A. Ferraro, Human adipose stem cells: from bench to bedside, Tissue Eng. B Rev. 21 (6) (2015) 572–584.
[28] N.E. Toledano Furman, Y. Lupu-Haber, T. Bronshtein, L. Kaneti, N. Letko, E. Weinstein, L. Baruch, M. Machluf, Reconstructed stem cell nanoghosts: a natural tumor targeting platform, Nano Lett. 13 (7) (2013) 3248–3255.
[29] F.H. Moonschi, A.K. Effinger, X. Zhang, W.E. Martin, A.M. Fox, D.K. Heidary, J.E. DeRouchey, C.I. Richards, Cell-derived vesicles for single-molecule imaging of membrane proteins, Angew. Chem. 127 (2) (2015) 491–494.
[30] B.T. Luk, C.-M.J. Hu, R.H. Fang, D. Dehaini, C. Carpenter, W. Gao, L. Zhang, Interfacial interactions between natural RBC membranes and synthetic polymeric nanoparticles, Nanoscale 6 (5) (2014) 2730–2737.
[31] J. Shi, Z. Xiao, A.R. Votruba, C. Vilos, O.C. Farokhzad, Differentially charged hollow core/shell lipid–polymer–lipid hybrid nanoparticles for small interfering RNA delivery, Angew. Chem. 123 (31) (2011) 7165–7169.
[32] R.J. Bose, S.-H. Lee, H. Park, Lipid polymer hybrid nanospheres encapsulating antiproliferative agents for stent applications, J. Ind. Eng. Chem. 36 (2016) 284–292.
[33] G.S. Teo, J.A. Ankrum, R. Martinelli, S.E. Boetto, K. Simms, T.E. Sciuto, A.M. Dvorak, J.M. Karp, C.V. Carman, Mesenchymal stem cells transmigrate between and directly through tumor necrosis factor-α-activated endothelial cells via both leukocyte-like and novel mechanisms, Stem Cell. 30 (11) (2012) 2472–2486.
[34] O. Lunov, T. Syrovets, C. Loos, J. Beil, M. Delacher, K. Tron, G.U. Nienhaus, A. Musyanovych, V. Mailander, K. Landfester, Differential uptake of functionalized polystyrene nanoparticles by human macrophages and a monocytic cell line, ACS Nano 5 (3) (2011) 1657–1669.
[35] R. Nagaya, M. Mizuno-Kamiya, E. Takayama, H. Kawaki, I. Onoe, T. Tanabe, K. Nagahara, N. Kondoh, Mechanisms of the immunosuppressive effects of mouse adipose tissue-derived mesenchymal stromal cells on mouse alloreactively stimulated spleen cells, Experimental and therapeutic medicine 7 (1) (2014) 17–22.
[36] G. Qiu, G. Zheng, M. Ge, L. Huang, H. Tong, P. Chen, D. Lai, Y. Hu, B. Cheng, Q. Shu, Adipose-derived mesenchymal stem cells modulate CD14+ + CD16+ expression on monocytes from sepsis patients in vitro via prostaglandin E2, Stem Cell Res. Ther. 8 (1) (2017) 97.

[37] F. Gao, S. Chiu, D. Motan, Z. Zhang, L. Chen, H. Ji, H. Tse, Q.-L. Fu, Q. Lian, Mesenchymal stem cells and immunomodulation: current status and future prospects, Cell Death Dis. 7 (1) (2017) e2062.
[38] F. Yang, S.-W. Cho, S.M. Son, S.R. Bogatyrev, D. Singh, J.J. Green, Y. Mei, S. Park, S.H. Bhang, B.-S. Kim, Genetic engineering of human stem cells for enhanced angiogenesis using biodegradable polymeric nanoparticles, Proc. Natl. Acad. Sci. Unit. States Am. 107 (8) (2010) 3317–3322.
[39] J. Kim, L. Cao, D. Shvartsman, E.A. Silva, D.J. Mooney, Targeted delivery of nanoparticles to ischemic muscle for imaging and therapeutic angiogenesis, Nano Lett. 11 (2) (2010) 694–700.
[40] C. Tu, S. Das, A.B. Baker, J. Zoldan, L.J. Suggs, Nanoscale strategies: treatment for peripheral vascular disease and critical limb ischemia, ACS Nano 9 (4) (2015) 3436–3452.
[41] L. Deveza, J. Choi, J. Lee, N. Huang, J. Cooke, F. Yang, Polymer-dna nanoparticle-induced CXCR4 overexpression improves stem cell engraftment and tissue regeneration in a mouse hindlimb ischemia model, Theranostics 6 (8) (2016) 1176.
[42] R.J. Bose, R. Paulmurugan, J. Moon, S.-H. Lee, H. Park, Cell membrane-coated nanocarriers: the emerging targeted delivery system for cancer theranostics, Drug Discov. Today (2018).